iScience

CellPress
OPEN ACCESS

Article

Unusual (2*R*,6*R*)-bicyclo[3.1.1]heptane ring construction in fungal *α*-*trans*-bergamotene biosynthesis

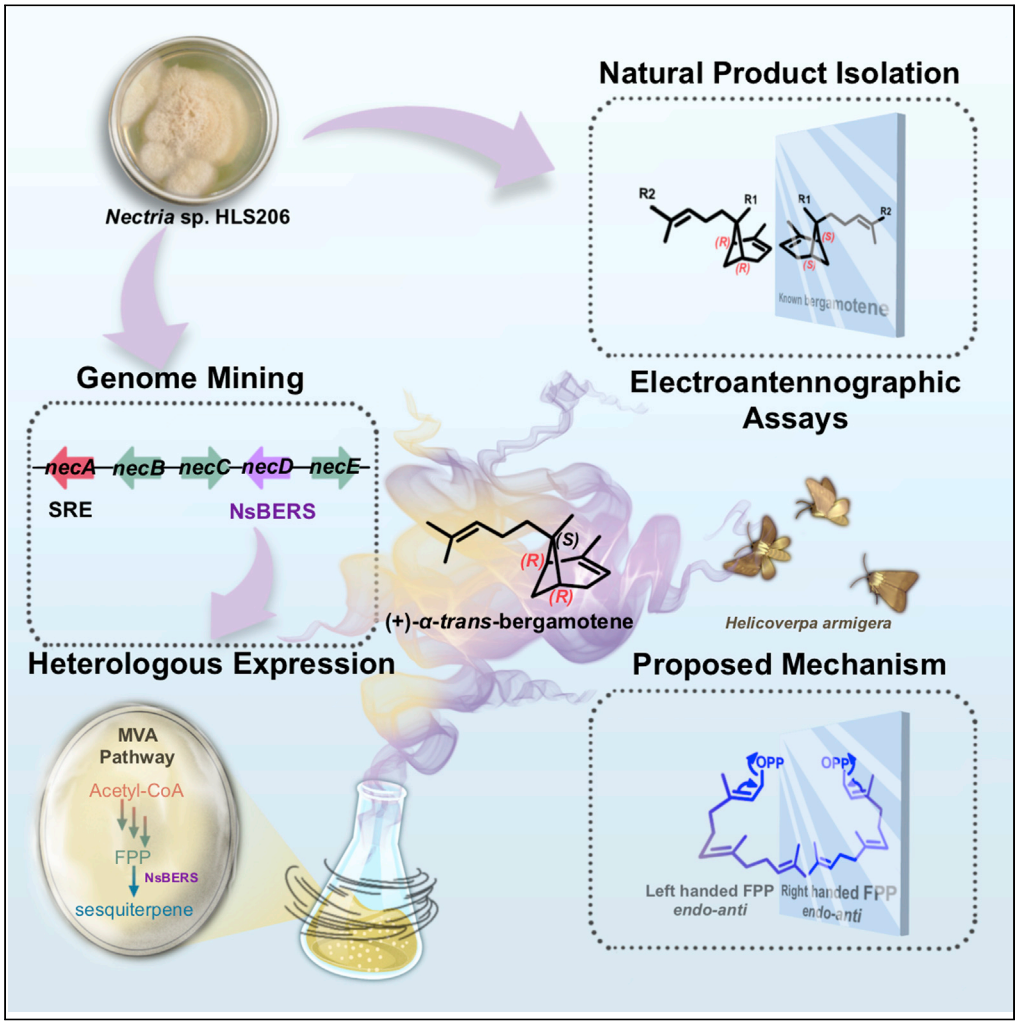

Yan-Hua Wen, Tian-Jiao Chen, Long-Yu Jiang, ..., Rui-Shan Wang, Ting Gong, Ping Zhu

gongting@imm.ac.cn (T.G.)
zhuping@imm.ac.cn (P.Z.)

Highlights

Bergamotene derivatives with unusual (2*R*,6*R*) configurations from marine fungus

(+)-*α*-*trans*-bergamotene synthase NsBERS as a gateway to identify LsBERS and BcBOS

The *endo-anti* cyclization of left-handed helix FPP involving (6*R*)-bisabolyl cation

Volatiles elicited significant EAG responses suggesting their biocontrol potential

Wen et al., iScience *25*, 104030
April 15, 2022
https://doi.org/10.1016/j.isci.2022.104030

iScience

CellPress
OPEN ACCESS

Article

Unusual (2*R*,6*R*)-bicyclo[3.1.1]heptane ring construction in fungal α-*trans*-bergamotene biosynthesis

Yan-Hua Wen,[1] Tian-Jiao Chen,[1] Long-Yu Jiang,[1] Li Li,[1] Mengbo Guo,[2] Yu Peng,[1] Jing-Jing Chen,[1] Fei Pei,[1] Jin-Ling Yang,[1] Rui-Shan Wang,[1] Ting Gong,[1,*] and Ping Zhu[1,3,*]

SUMMARY

Bergamotenes are bicyclo[3.1.1]heptane sesquiterpenes found abundantly in plants and fungi. Known bergamotene derivatives all possess (2*S*,6*S*)-bergamotene backbone. In this study, two (+)-α-*trans*-bergamotene derivatives (1 and 2) with unusual (2*R*,6*R*) configuration were isolated and elucidated from marine fungus *Nectria* sp. HLS206. The first (+)-α-*trans*-bergamotene synthase NsBERS was characterized using genome mining and heterologous expression-based strategies. Based on homology search, we characterized another (+)-α-*trans*-bergamotene synthase LsBERS from *Lachnellula suecica* and an (+)-α-bisabolol synthase BcBOS from *Botrytis cinerea*. We proposed that the cyclization mechanism of (+)-α-*trans*-bergamotene involved *endo-anti* cyclization of left-handed helix farnesyl pyrophosphate by (6*R*)-bisabolyl cation, which was supported by molecular docking. The biosynthesis-based volatiles (3–6) produced by heterologous fungal expression systems elicited significant electroantennographic responses of *Helicoverpa armigera* and *Spodoptera frugiperda*, respectively, suggesting their potential in biocontrol of these pests. This work enriches diversity of sesquiterpenoids and fungal sesquiterpene synthases, providing insight into the enzymatic mechanism of formation of enantiomeric sesquiterpenes.

INTRODUCTION

Terpenoids are derived from C5 isoprene units and possess intriguing structural diversity (Christianson, 2008). More than 80,000 terpenoids have been identified to date (Christianson, 2017). Sesquiterpenoids represent the largest subgroup of terpenoids which have varied applications in pharmaceutical (e.g. artemisinin), biofuels (e.g. farnesene and bisabolene), flavor (e.g. carotenoids), and fragrance (e.g. nerolidol) industries (Miller and Allemann, 2012; Peralta-Yahya et al., 2011). As the well-known constituents of plant essential oils, bergamotenes are a type of bicyclic sesquiterpenes. Some bioactive bergamotene lactones such as massarinolin A (Oh et al., 1999), expansolides C and D (Ying et al., 2017), and purpurolides A and B (Wang et al., 2018) have been isolated from fungi. In the last few decades, bergamotene-type sesquiterpenes having backbones with (2*S*,6*S*,7*R*/*S*) absolute configuration derived from (6*S*)-bisabolyl cation have been described and important examples include (−)-α-*trans*/*cis*-bergamotene and β-*trans*/*cis*-bergamotene (Cane et al., 1990b; Coates et al., 1988; Gibson and Erman, 1969). In this study, we isolated two new (+)-α-*trans*-bergamotene derivatives **1** and **2** from marine fungus *Nectria* sp. HLS206. These compounds possess unusual (2*R*,6*R*) absolute configurations, which challenged the concept that bergamotene skeleton was exclusively cyclized from (6*S*)-bisabolyl cation (Li et al., 2019; Sallaud et al., 2009).

In contrast to the increasing number of terpenoids being reported, the characterization of terpene synthases (TPSs) is yet to be explored comprehensively. Nevertheless, in the post-genomic era, the blossoming of sequencing technology and bioinformatics provides the opportunity for the identification of fungal TPSs. The active site contour of TPS serves as a template for catalysis, ensuring that the substrate adopts proper conformation yielding the correct product by complex cascade reaction (Christianson, 2017; Tantillo, 2011). Known fungal sesquiterpene synthases (STSs) mainly belong to class I TPSs which catalyze an ionization-dependent cyclization of farnesyl diphosphate (FPP) and are characterized by signature metal binding motifs DDXXD and NSE which are located on helix D and helix H, respectively (Christianson, 2017).

[1]State Key Laboratory of Bioactive Substance and Function of Natural Medicines; NHC Key Laboratory of Biosynthesis of Natural Products; CAMS Key Laboratory of Enzyme and Biocatalysis of Natural Drugs, Institute of Materia Medica, Chinese Academy of Medical Sciences & Peking Union Medical College, Beijing 100050, China

[2]State Key Laboratory for Biology of Plant Diseases and Insect Pests, Institute of Plant Protection, Chinese Academy of Agricultural Sciences, Beijing 100193, China

[3]Lead contact

*Correspondence: gongting@imm.ac.cn (T.G.), zhuping@imm.ac.cn (P.Z.)

https://doi.org/10.1016/j.isci.2022.104030

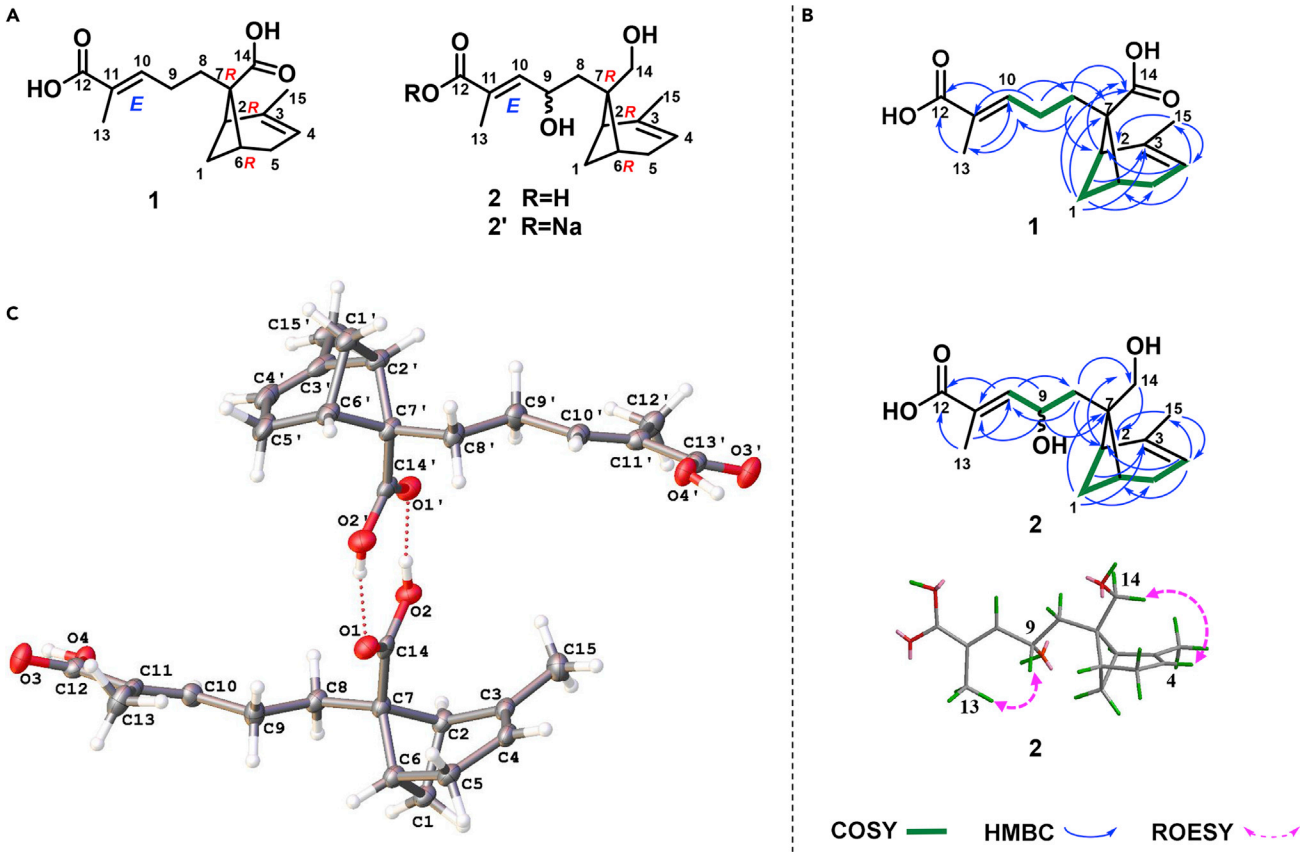

Figure 1. Structure elucidation of compounds 1, 2 and 2′ isolated from the marine fungus *Nectria* sp. HLS206

(A–C) (A) Structures of compounds **1**, **2** and **2′**; (B) Key COSY, HMBC and ROESY correlations of **1** and **2**; (C) X-Ray ORTEP drawing of **1**.

So far, several plant-derived promiscuous bergamotene synthases belonging to soluble class I TPSs have been identified (Jones et al., 2011; Landmann et al., 2007; Sallaud et al., 2009). However, the only identified fungal bergamotene synthase Fma-TC (*β-trans*-bergamotene synthase) best known for its significant role in the biosynthesis of fumagillin belongs to the UbiA superfamily (Lin et al., 2013). To the best of our knowledge, no fungal (−)-*α-trans*-bergamotene synthase has been characterized to date, let alone (+)-*α-trans*-bergamotene synthase. To get more insight into this kind of enzyme and to understand its enzymatic mechanism, we sequenced the whole genome of *Nectria* sp. HLS206. By genome mining and heterologous expression strategies, we found and characterized the first (+)-*α-trans*-bergamotene synthase NsBERS (NecD). Upon sequencing and phylogenetic analysis, we identified another (+)-*α-trans*-bergamotene synthase LsBERS (GenBank: TVY81921.1) and BcBOS (GenBank: XP_001546971.2) that produced (3*R*)-nerolidol and (+)-*α*-bisabolol with unusual configurations. We proposed that the enzymatic mechanism involved *endo-anti* cyclization of a left-handed helix FPP, which was supported by molecular docking.

RESULTS

Isolation and structure elucidation of new bergamotene derivatives necbergamotenoic acids A and B

Two new (+)-*α-trans*-bergamotene derivatives with unusual (2*R*,6*R*) configurations named necbergamotenoic acid A (**1**) and necbergamotenoic acid B (**2**, its ionized form **2′**) were isolated from marine *Nectria* sp. HLS206 (Figure 1A), and their structures were elucidated by a combination of NMR (Figure 1B) and X-ray diffraction analysis (Figure 1C).

Necbergamotenoic acid A (**1**), colorless crystals with $[\alpha]_D^{20}$ +51.5 (*c* 0.2, CH_3OH), had the molecular formula $C_{15}H_{20}O_4$ based on HRESIMS data (*m/z* 287.1246 $[M + Na]^+$, calcd for $C_{15}H_{20}O_4Na$, 287.1254, Figure S8),

Table 1. The ^{1}H NMR (500 MHz) and ^{13}C NMR (125 MHz) data of necbergamotenoic acid A (1), necbergamotenoic acid B (2) and its ionized form (2′)

	1[a]		2[b]		2′[b]	
No	δ_H mult. (*J* in Hz)	δ_C	δ_H mult. (*J* in Hz)	δ_C	δ_H mult. (*J* in Hz)	δ_C
1a	1.28, d (8.0)	29.7	1.23, d (8.5)	31.9	1.21, d (8.0)	32.0
1b	2.28, dd (8.0, 6.0)		2.38, dd (8.5, 6.0)		2.36, m	
2	2.26, d (6.0)	43.5	2.30, m	44.0	2.30–2.32[c], m	43.8
3		146.1		145.0		145.0
4	5.15, brs	116.5	5.27, d (1.5)	117.8	5.26, brs	117.9
5a	2.61, m	31.7	2.20, m	31.9	2.20, m	32.0
5b			2.24, m		2.23, m	
6	2.57, m	39.3	2.36, m	41.0	2.30–2.32[c], m	41.2
7		52.9		45.0		45.0
8a	2.15, brt (6.0)	33.4	1.95, dd (15.0, 3.5)	42.2	1.95, dd (15.0, 4.0)	42.8
8b			2.05, dd (15.0, 9.5)		1.98, dd (15.0, 8.5)	
9	2.37, m	24.9	4.70, ddd (9.5, 8.5, 3.5)	67.1	4.63, ddd (9.5, 8.5, 4.0)	67.3
10	6.81, t (6.0)	144.9	6.74, dq (8.5, 1.0)	145.9	6.53, dq (9.5, 1.0)	141.1
11		128.0		128.3		133.7
12		173.7		171.6		177.6
13	1.78, s	12.2	1.88, d (1.0)	12.8	1.87, d (1.0)	14.1
14a		181.6	3.72, d (10.5)	63.7	3.71, d (10.5)	63.9
14b			3.37, d (10.5)		3.30, d (10.5)	
15	1.71, d (1.0)	22.6	1.73, d (1.5)	22.8	1.73, d (1.5)	22.8

[a]Recorded in $CDCl_3$.
[b]Recorded in CD_3OD.
[c]Overlapped.

indicating six degrees of unsaturation. Analysis of the ^{1}H, ^{13}C and heteronuclear single quantum coherence (HSQC) NMR data (Table 1, Figures S10–S12) revealed the presence of two methyl groups, four methylene carbons, four methine carbons (which included two olefinic methine carbons), and five quaternary carbons (which included two disubstituted olefinic carbons and two carboxyl carbons). These results indicated that compound **1** might be a sesquiterpene containing two rings with two double bonds and two carboxylic acid groups. The heteronuclear multiple bond correlations (HMBCs) from H-4 to C-2, C-6 and C-15, from 15-CH_3 to C-2 and C-4, from H-1a/1b to C-3 and C-5, from H-1a to C-14, from H-2 to C-4 and C-15 (Figure S13), suggested that compound **1** was α-bergamotane sesquiterpene with bicyclo[3.1.1]heptane ring (Oh et al., 1999), in which 14-CH_3 was oxygenated into carboxylic acid. Besides, HMBCs from 13-CH_3 to C-10, C-11 and C-12, from H-10 to C-8, C-12 and C-13, from H-9 to C-7 and C-11, from H-8 to C-2, C-6, C-10 and C-14, indicated the presence of α,β-unsaturated carboxylic acid group in the side chain (Figures 1B and S13). The double bond between C-10 and C-11 was assigned as *E* geometry based on the strong rotating frame overhauser effect spectroscopy (ROESY) correlation between H-9 and 13-CH_3 (Figure S15). The homonuclear correlation spectroscopy (COSY) spectrum (Figures 1B and S14) revealed two spin systems (-^{4}CH^{5}CH$_2$^{6}CH^{1}CH$_2$^{2}CH- and -^{8}CH$_2$^{9}CH$_2$^{10}CH-), which further elucidated the planar structure of **1** as shown in Figure 1A. The single crystals of **1** were generated, and X-ray crystallography was performed subsequently using Gu Kα radiation, which confirmed the structure and determined the absolute configuration of 1 (*2R,6R,7R*) (Figure 1C, Table S1). To our knowledge, this is the first time that a natural bergamotene derivative in this configuration has been identified.

Necbergamotenoic acid B (**2**) was obtained as yellowish gum with $[\alpha]^{20}_{D}$ +100.9 (*c* 0.2, CH_3OH), and its molecular formula was established as $C_{15}H_{22}O_4$ on the basis of HRESIMS at *m/z* 289.1405 $[M + Na]^+$ (calcd for $C_{15}H_{22}O_4Na$, 289.1410, Figure S17), requiring five degrees of unsaturation. Compared with the ^{1}H NMR and ^{13}C NMR spectra of compound **1**, one oxygenated methine signal at δ_H 4.70, δ_C 67.1, two oxygenated methylene signals at δ_H 3.72, 3.37, δ_C 63.7 appeared and one carboxyl carbon signal at δ_C 181.6 was missing (Table 1, Figures S19–S21), which indicated the presence of two hydroxyl groups in the α-bergamotenoic

acid. Further analysis of COSY and HMBC spectra determined the hydroxyl groups were assigned to C-9 and C-14 (Figures 1B, S22 and S23). The relative stereochemistry of the skeleton of compound **2** was determined as (10*E*)-α-*trans*-bergamotenoic acid based on ROESY correlations (Figures S24) between H-14a/H-4 and H-9/13-CH_3, which was the same as **1**. Since the qualified crystals of **2** were not obtained and any useful information could not be acquired by Mosher's method, we deduced the absolute configuration of the skeleton of **2** as 2*R*,6*R*,7*R* based on the biosynthetic pathway, but the absolute configuration of C-9 is still waiting for the determination (Figure 1A).

The ionized form of necbergamotenoic acid B (**2′**) was also isolated as a yellowish gum. Its HRESIMS spectrum showed the positive ion peak at *m/z* 289.1403 (calcd for $C_{15}H_{22}O_4Na$, 289.1410, Figure S26), which was the same as that of **2**. In the IR spectrum of **2′** (Figure S27), the carbonyl group had two bands situated at 1573 and 1426 cm^{-1} that are typical of ionized groups ($RCOO^-$) (Max and Chapados, 2004). On basis of 1D NMR (^1H and ^{13}C NMR, Table 1, Figures S28, S29 and 2D NMR (HSQC, HMBC, COSY and ROESY, Figures S30–S33) spectra, the structure of **2′** was confirmed and all the ^1H and ^{13}C NMR chemical shifts were assigned as Table 1. The carbon signals of C-11 and C-12 for α,β-unsaturated carboxylic acid group in ionized form (**2′**) shifted downfield about 5 ppm, which was consistent with the results reported in the literature (Cistola et al., 1982).

The sesquiterpenome of *Nectria* sp. HLS206

To explore how α-*trans*-bergamotene was synthesized in fungi, specifically (+)-α-*trans*-bergamotene, the whole genome of *Nectria* sp. HLS206 was sequenced and submitted to anti-SMASH 4.0 (Blin et al., 2017) for prediction of terpene biosynthetic gene clusters (BGCs). Excluding prenyltransferases and squalene synthases, only two candidate STSs (Nec04 and Nec26) were predicted. However, no oxidative tailoring enzyme was found adjacent to them. Using local BLAST with over 50 fungal STSs probes, another candidate sesquiterpene synthase NecD (scaffold 23) was mined although it was targeted by only a few probes with low identities/positives (~25%/45%). The gene annotation of upstream and downstream of *necD* revealed three cytochrome P450 monooxygenases (NecB, NecC and NecE), which could be responsible for the oxidation from (+)-α-*trans*-bergamotene to **1** and **2** (Figure 2A, Table S4). Furthermore, *necA* encodes a p53 inducible quinone oxidoreductase PIG3 involving cellular responses to oxidative stress (Porte et al., 2009) which seemed to be a self-resistance enzyme (SRE). As a result, we hypothesized that NecD may be responsible for the biosynthesis of (+)-α-*trans*-bergamotene skeleton.

The *Aspergillus nidulans* host system has been proved to be capable of heterologous terpene production. To verify our above-mentioned hypothesis, we cloned *nec04*, *nec26* and *necD* genes from HLS206 gDNA and conducted heterologous expression in *A. nidulans* for functional analysis. The organic layers covering on the fermentation were analyzed by GC-MS. In comparison with the mock transformant, the sole product of *AN-necD* at 9.9 min (**3**) and the main product of *AN-nec26* at 12.9 min (**4**) were identified as bergamotene and trichoacorenol by NIST library respectively, while no new product was found in *AN-nec04* (Figure 2B).

Compounds **3** and **4** were purified from *AN-necD* and *AN-nec26* fermentation, respectively, and their structures were determined using NMR spectroscopy. The NMR data of **4** (Table S3, Figures S38 and S39) were consistent with reported data of trichoacorenol and $[\alpha]^{20}_D$ −6 (*c* 0.1, $CHCl_3$) of **4** was consistent with previous study $[\alpha]^{20}_D$ −5.2 (*c* 0.12, $CHCl_3$) (Brock and Dickschat, 2011). Thus **4** was assigned as (−)-trichoacorenol and Nec26 was defined as NsTAS. The cyclization mechanism of (−)-trichoacorenol has been elaborated in a recent study (Rinkel and Dickschat, 2020).

By comparing the NMR data (Table S2, Figures S35 and S36) with the reported data (Sy and Brown, 1997), the relative structure of **3** was identified as α-*trans*-bergamotene consistent with that of compound **1**. Furthermore, the specific rotation of **3** was positive and opposite to that of (−)-α-*trans*-bergamotene (Chapuis et al., 1998), implying that the absolute configuration of **3** was 2*R*,6*R*,7*S* (Figure 2B). The positive cotton effect at 209 nm of **3** was contrary to that of (−)-*S*-α-pinene in the CD spectrum (Figure S37) (Mason and Schnepp, 1973), further proving that the absolute configuration of **3** was consistent with that of **1**. To the best of our knowledge, this is the first report of (+)-α-*trans*-bergamotene skeleton.

NsBERS converts (2*E*,6*E*)-FPP to (+)-α-*trans*-bergamotene

In comparison with the only known fungal bergamotene synthase Fma-TC with transmembrane helices, the NecD (hereby named NsBERS) was a 435-amino-acid protein containing the aspartate-rich motif

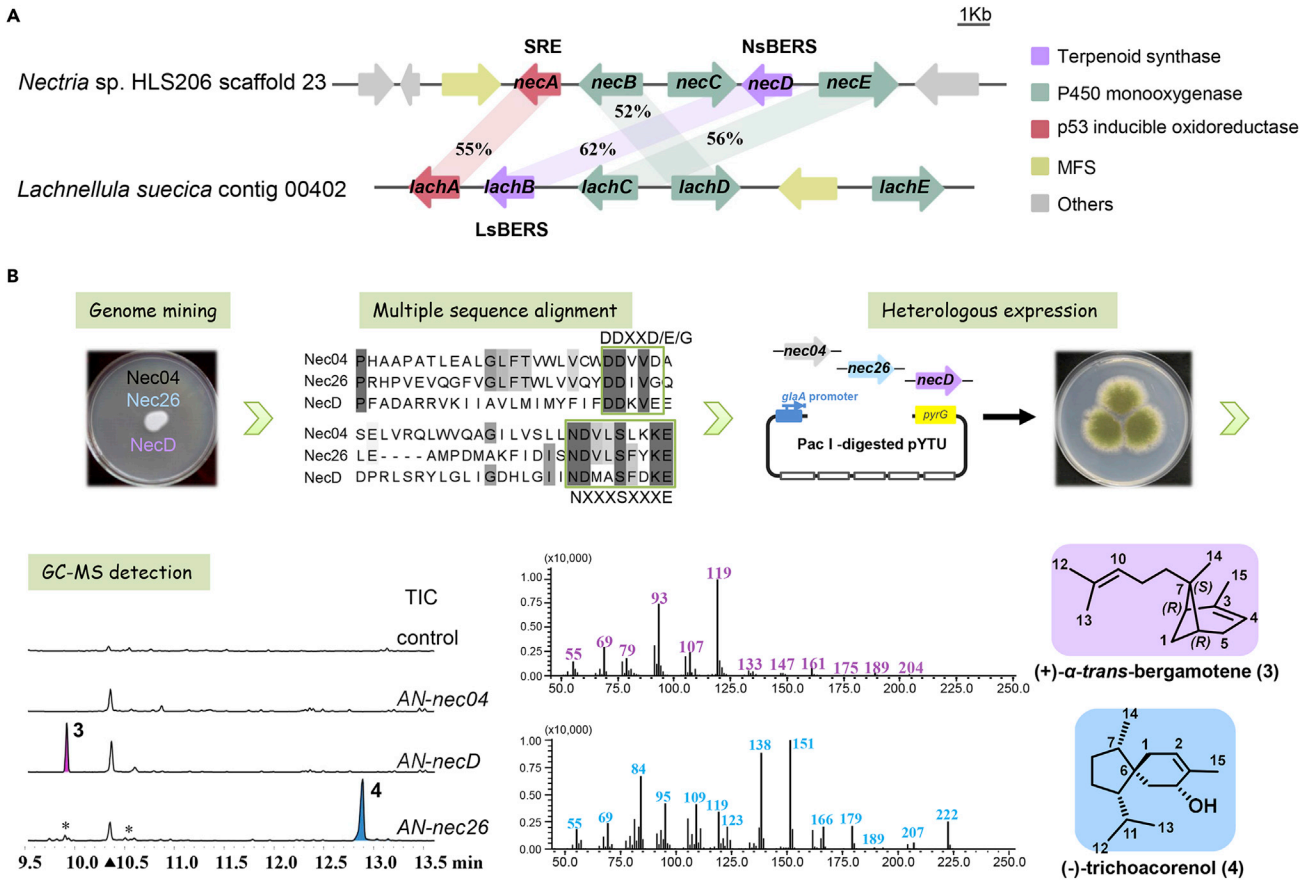

Figure 2. The sesquiterpenome of *Nectria* sp. HLS206

(A and B) (A) Schematic representation of the *nec* and *lach* gene clusters and their amino acid sequence identity (The genes *necD* and *lachB* encode NsBERS and LsBERS, respectively); (B) The mining and identification of STSs in *Nectria* sp. HLS206. The *n*-dodecane layers of *AN-nec04*, *AN-necD* and *AN-nec26* expressed strains were analyzed by GC-MS. The asterisks represent minor products of *AN-nec26* and the triangle represents dodecanol at 10.35 min.

(DDXXD/E), NSE motif and R, RY sensors (Figure S5), which are usually conserved in class I terpene synthases. By fusion with N-terminal MBP-His_6 tag, the soluble fusion protein (91 kDa) was acquired by affinity chromatography (Figure S1). Incubation of NsBERS with FPP and Mg^{2+} resulted in the formation of sole product **3** (Figure S2). Additionally, Mn^{2+} and Co^{2+} can also be used as the cofactors of NsBERS and the optimal concentration of divalent metal ion was tested (Figure S3). The enzyme activity was insensitive to the concentration of Mg^{2+} (at the range from 0.005 mM to 500 mM). The total amount of product reached a maximum at concentrations of 0.2 mM Mn^{2+} and 1 mM Co^{2+}, while higher concentrations led to activity loss. Substrate promiscuity assay showed that NsBERS cannot accept GPP and GGPP as substrates (Figure S4).

Phylogenetic analysis of fungal STSs and the NsBERS-like subclade

The exhaustive work by Schmidt-Dannert's group has demonstrated the correlation between clade and cyclization mechanism in basidiomycetes STSs (clade I and clade IV) (Figure 3) (Agger et al., 2009; Wawrzyn et al., 2012), and has been seminal in guiding the development of in silico approaches for the directed discovery of new STSs with a specific cyclization mechanism (Quin et al., 2014; Zhang et al., 2020). However, the dispersive and unsystematic identifications reported till date do not allow cyclization mechanism or product type prediction rules to be set in place for ascomycetes STSs.

As the first identified (+)-α-*trans*-bergamotene synthase, NsBERS shares the same initial 1,6 cyclization mechanism as NsTAS in clade IV (Figure 3). However, the clade IV conserved in 1,6 cyclization is predominantly constituted by basidiomycetes STSs than ascomycetes STSs and genes in clade IV seem to be involved in horizontal gene transfer from basidiomycetes to ascomycetes. NsBERS is away from

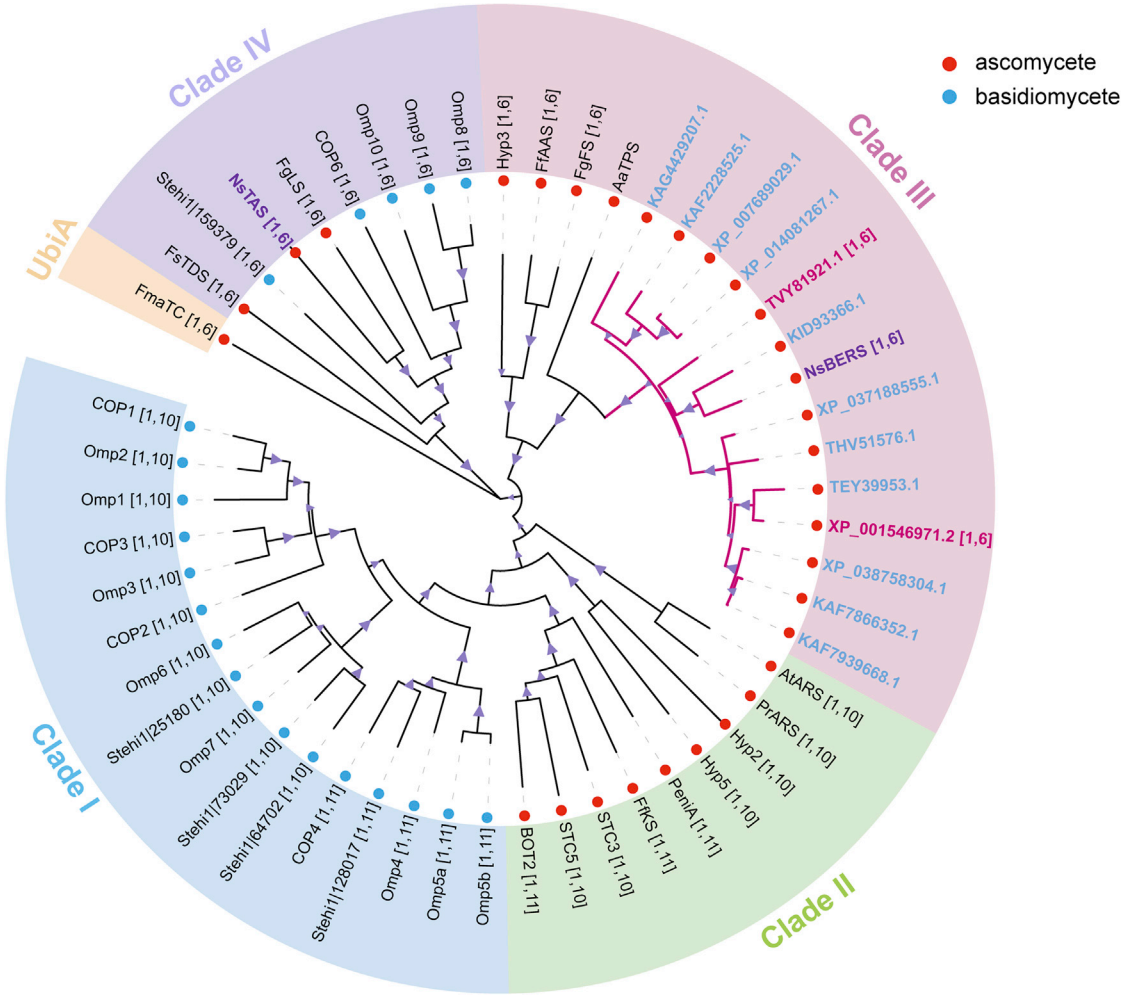

Figure 3. Phylogenetic analysis of fungal sesquiterpene synthases

Fma-TC of UbiA superfamily was chosen as the outgroup. Branches are labeled with triangles representing the percentage of 1000 bootstrap replicates. The initial cyclization mechanism catalyzed by identified enzymes are indicated in square brackets. Hyp3 (1,8-cineole synthase) from *Hypoxylon* sp. in clade III is the first identified fungal monoterpene synthase and its mutants N136S and N136A can yield sesquiterpene products. TVY81921.1 corresponds to LachB in Figure 2A.

this clade and located in clade III in which FgFS (Bian et al., 2018), FfAAS (Brock et al., 2013) and Hyp3 (Shaw et al., 2015) also exhibited 1,6 cyclization but shared only ~26% identity with NsBERS (Figure S5). This phenomenon signified that there must exist STSs which are more phylogenetically related to NsBERS, therefore NsBERS may have the potential to facilitate the discovery of relevant fungal STSs. We performed a homology search in NCBI and got a set of uncharacterized NsBERS homologues belonging to the genera of *Botrytis*, *Bipolaris*, *Metarhizium*, *Lachnellula*, and so on separately (Table S6). After redundancy removal, the sequences with over 45% identity with NsBERS were chosen to analyze the phylogenetic relation, and a new subclade was formed (Figure 3). We hypothesized that this NsBERS-like subclade may well possess a similar cyclization mechanism and form similar products.

NsBERS serves as a gateway to identify LsBERS and BcBOS

To verify our hypothesis, TVY81921.1 from *Lachnellula suecica* (Giroux and Bilodeau, 2020) and XP_001546971.2 described as Bcstc4 from *Botrytis cinerea* B05.10 (Van Kan et al., 2017) (Figure 3, Table S6) were chosen for fast identification in *Saccharomyces cerevisiae*. As the key enzymes in mevalonate (MVA) pathway, HMGR, and FPP synthase (ERG20) were overexpressed to produce sufficient FPP for the production of sesquiterpenoids (Figure 4A). The GC-MS analysis of the organic layers covering the

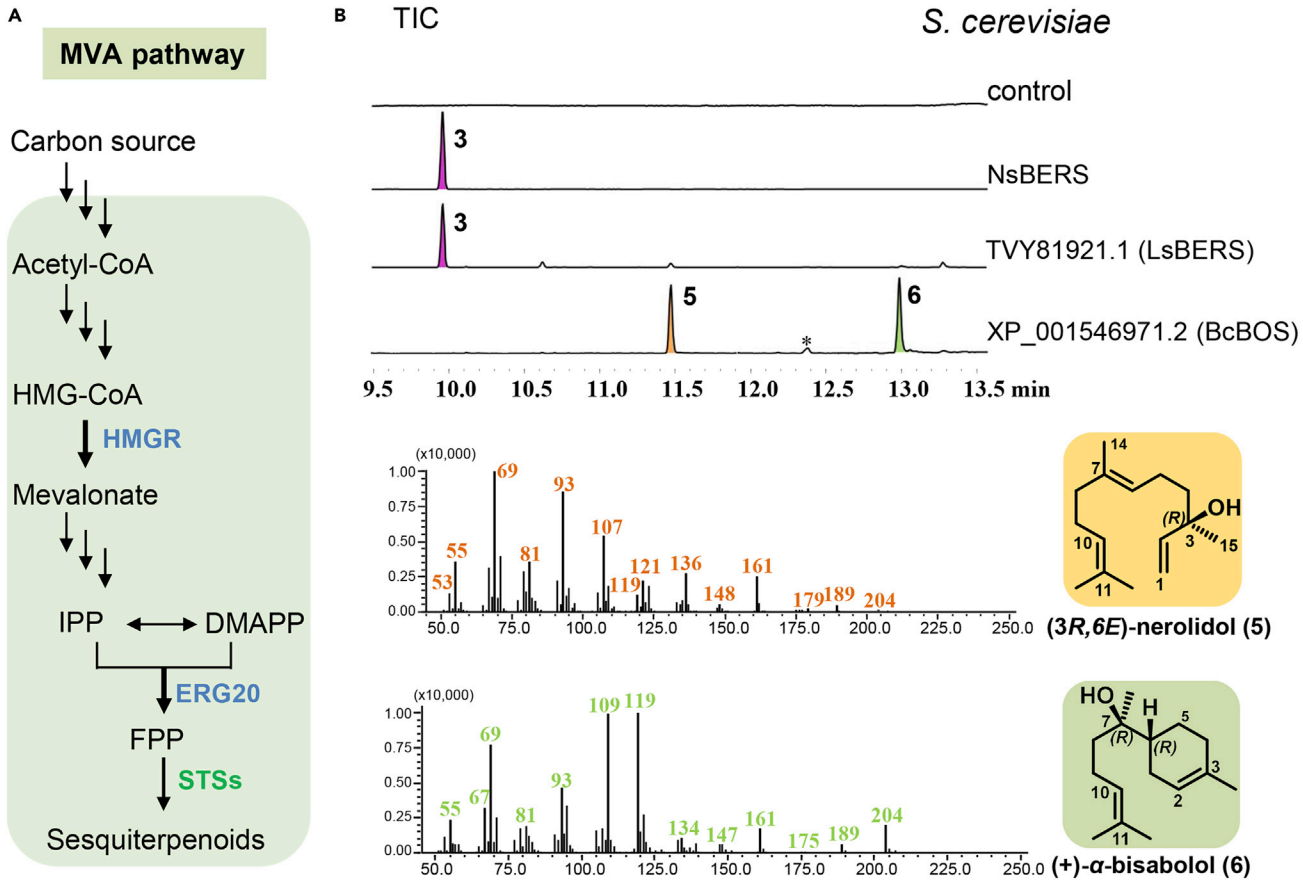

Figure 4. Heterologous expression of NsBERS-like STSs (NsBERS, TVY81921.1 and XP_001546971.2) in *S. cerevisiae* BJ5464

(A) Schematic representation of the engineered sesquiterpenoid biosynthetic pathway in *S. cerevisiae*. The key enzymes HMGR and ERG20 were overexpressed to produce sufficient FPP for the production of sesquiterpenoids.

(B) The function characterization of TVY81921.1 and XP_001546971.2. The *n*-octane layers of *S. cerevisiae* engineered strains were analyzed by GC-MS. The asterisks represent minor product of XP_001546971.2.

fermentation broth revealed that the product retention time of TVY81921.1 was consistent with that of NsBERS, while XP_001546971.2 mainly generated *trans*-nerolidol (47%), α-bisabolol (52%) and a minor product (Figure 4B).

Further NMR analysis (Table S2) and the specific rotation indicated that the product of TVY81921.1 was (+)-α-*trans*-bergamotene ($[\alpha]^{20}_{D}$ +20 (*c* 0.06, $CHCl_3$)). Compound **5** (Table S3, Figures S40 and S41) was (3*R*,6*E*)-nerolidol ($[\alpha]^{20}_{D}$ −16 (*c* 0.1, $CHCl_3$)), and its specific rotation was consistent with $[\alpha]^{23}_{D}$ −12.5 (*c* 0.022, $CHCl_3$) (Cane et al., 1990a). Compound **6** (Table S3, Figures S42 and S43) was (+)-α-bisabolol ($[\alpha]^{20}_{D}$ +51.7 (*c* 0.06, $CHCl_3$)), and the NMR data of which were different from those of *epi*-α-bisabolol (Chen et al., 2002) and its specific rotation was sufficiently close to the reported $[\alpha]^{22}_{D}$ +51.3 (*c* 0.06, $CHCl_3$) (Bian et al., 2018; Gnther et al., 1993). Thus, TVY81921.1 as the second (+)-α-*trans*-bergamotene synthase was named as LsBERS, and XP_001546971.2 was designated as BcBOS which is the first identified fungal (+)-α-bisabolol synthase. Although (3*R*)-nerolidol and (+)-α-bisabolol were deemed to occur rarely as a constituent of natural products (Laurini et al., 2020), some related STSs derived from plants have been reported recently. For instance, the reports of maize TPS1 producing ~29% (3*R*)-nerolidol (Schnee et al., 2002) and several (+)-α-bisabolol synthases from the genus *Artemisia* (Muangphrom et al., 2016, 2019) indicated the lack of comprehensive studies in the domain of sesquiterpene enantiomers.

LsBERS exhibited the same properties as NsBERS, and the *in vitro* assay of the 92 kDa soluble fusion protein also contributed to the formation of **3** (Figure S3). However, the ratio of BcBOS products was influenced by

many factors such as the type and concentration of metal cofactor (Lopez-Gallego et al., 2010). The higher ratio of linear nerolidol can be detected *in vitro* when Mg^{2+} is used as the cofactor. Substitution of Mg^{2+} with Co^{2+} shifted the product profile to a higher (+)-α-bisabolol ratio, and higher concentration of Co^{2+} can contribute to higher ratio of cyclization product, implying that metal coordination interactions may play a significant role in governing the substrate binding conformation prior to the initiation of cyclization cascade (Christianson, 2017).

The proposed mechanism of (+)-α-*trans*-bergamotene

At this point in the study, NsBERS, LsBERS and BcBOS, which produced sesquiterpene backbones with unusual absolute configurations were characterized. Apparently, the C6 of **3** and **6** did not participate in further rearrangements and retained their configurations, that is, (+)-α-*trans*-bergamotene and (+)-α-bisabolol were both derived from (6*R*)-bisabolyl cation. These enzymes can be good models for studying the formation of (6*R*)-bisabolyl cation and pursing the difference with (6*S*)-bisabolyl cation. A general stereochemical model for bicyclic monoterpene proposed by Croteau et al. (Croteau, 1987) has been applied to elucidate the conformation control of (+)-bornyl diphosphate synthase (Whittington et al., 2002), 1,8-cineole synthase (Kampranis et al., 2007), (±)-α-pinene synthases (Croteau and Satterwhite, 1989) and (±)-limonene synthases (Kumar et al., 2017), respectively. A more recent computational chemistry study investigating the mechanism of santalenes produced by santalene synthase (SaSSy) has illustrated that the (6*S*)-bisabolyl cation is formed via *endo-anti* cyclization in the right-handed helix of FPP (Jindal and Sunoj, 2012) which is similar to those of (−)-α-pinene synthase and (−)-limonene synthase. Although (6*R*)-bisabolyl cation is possibly formed via the *exo-anti* cyclization of the right-handed helix of FPP, it is unfavorable for the subsequent C2–C7 bond formation. Therefore, we hypothesized that the (6*R*)-bisabolyl cation formed adopts the mirror image via *endo-anti* cyclization in the left-handed helix of FPP during the cyclization of (+)-α-*trans*-bergamotene (Figure 5).

To verify the hypothesis, homology modeling of NsBERS was carried out by adopting AaTPS (PDB: 6LCD) as the template (He et al., 2020). The crystal structure of AaTPS only bound two Mg^{2+} and the DDXXD motif on the helix D was apparently away from the pyrophosphate (PPi), implying incomplete closure of the active site. Although this may lead to deviation in the position of PPi, the results of the molecular docking of (2*E*,6*E*)-FPP displayed almost consistent left-handed *endo-anti* conformation (Figure 5A). The alternative suitable substrate (3*R*)-NPP and the product (+)-α-*trans*-bergamotene also exactly resembled the predicted mechanism (Figures 5B and 5C). The bent contour of active cavity must play an important role in controlling the pre-folding state of the substrate, while sulfur-cation interaction (dative S → cation bonded state) (Dixit et al., 2017) may anchor the cation intermediate in a reactive conformation. Furthermore, LaBERS from *Lavandula angustifolia* (mainly producing (−)-α-*trans*-bergamotene with a ratio of 74%) was chosen to illustrate the symmetrical state (Figures 5D–5F), due to the fungus-derived (−)-α-*trans*-bergamotene synthase was still not identified. The stabilization effect of W263 and M280 on cation supported the right-handed conformation, but the vertical shape of active cavity cannot guarantee the formation of C2–C7 bond to its maximum extent, which led to formation of linear sesquiterpene byproducts.

Electroantennographic (EAG) responses of *H. armigera* and *S. frugiperda* to compounds 3–6

A large amount of evidence indicated that microbial volatiles are eco-friendly and have important applications in agricultural practices for sustainable development (Kanchiswamy et al., 2015). For instance, nerolidol has insecticidal activity (Chan et al., 2016) and has been reported as an important pheromone secreted by queens of higher termites (Havlickova et al., 2019). Hence, the EAG responses of *H. armigera* and *S. frugiperda* to biosynthesis-based volatiles (+)-α-*trans*-bergamotene (**3**), (−)-trichoacorenol (**4**), (3*R*,6*E*)-nerolidol (**5**) and (+)-α-bisabolol (**6**) were recorded. The results revealed that all of these volatiles can induce EAG responses (Figure 6). Especially, **5** elicited the highest responses of both *H. armigera* and *S. frugiperda*. To *H. armigera*, the EAG response values of females to (+)-α-*trans*-bergamotene were significantly higher than those of males, which suggested that **3** can attract female moths to oviposit (Figure 6A).

DISCUSSION

Polycyclic terpenoids usually have multiple chiral centers, and the chiral terpene pool has long served as the building blocks for chemical synthesis of complex natural products (Brill et al., 2017). However, a lot of sesquiterpenoids were identified only based on comparison of standards and NIST library, which overlooked the stereochemistry. In fact, it is essential to emphasize the pertinence of a more comprehensive

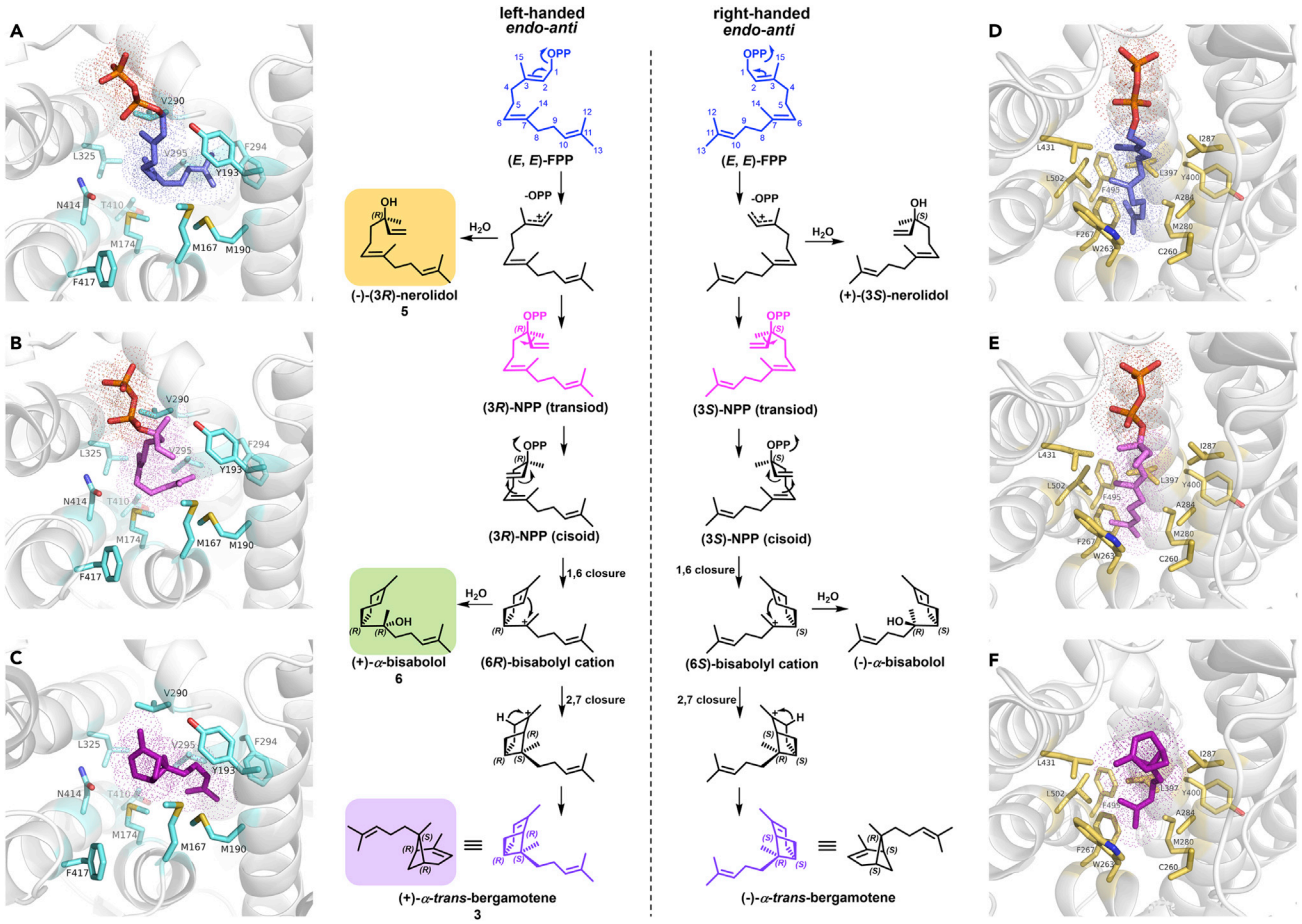

Figure 5. The proposed left-handed *endo-anti* cyclization mechanism of NsBERS, LsBERS and BcBOS

(A) (2*E*,6*E*)-FPP; (B) (3*R*)-NPP; and (C) (+)-α-*trans*-bergamotene were docked into NsBERS model, while (D) (2*E*,6*E*)-FPP; (E) (3*S*)-NPP; and (F) (−)-α-*trans*-bergamotene were docked into LaBERS model. The crystal structure of (4*S*)-limonene synthase complex (PDB: 2ONH) was used as the template for homology modeling of LaBERS.

understanding of stereochemistry of sesquiterpenoids, which will not only facilitate understanding the biogenesis of naturally occurring enantiomers but also will provide insight into enzymatic mechanism of precise stereochemistry control. In the last decades, bergamotene derivatives isolated from plants and fungi have been known to possess the (2*S*,6*S*) ring configurations. In this study, the isolation and identification of necbergamotenoic acids A and B (**1** and **2**) from marine fungus *Nectria* sp. HLS206 with (2*R*,6*R*) configurations broke this notion and enriched the chemical diversity of the bergamotene skeleton.

To investigate the biosynthetic mechanism, the whole genome of *Nectria* sp. HLS206 was sequenced and detailed bioinformatics-based analyses were carried out. By genome mining and heterologous expression in *A. nidulans*, we characterized the first (+)-α-*trans*-bergamotene synthase NsBERS with high fidelity. Upon homology search and phylogenetic analysis, we identified another (+)-α-*trans*-bergamotene synthase LsBERS and the first fungal (+)-α-bisabolol synthase BcBOS which indicated that NsBERS is a representative of untouched land and has the potential to facilitate discovery of relevant fungal STSs. The unusual stereochemistry of compounds **3**, **5** and **6** revealed that the structure elucidation of sesquiterpene enantiomers has been ignored to a degree. In addition, the disregard for NsBERS-like subclade proved that fungal STSs are still relatively unexplored and comprehensive studies designed to get a more in-depth understanding are pertinent. Furthermore, the phylogenetic analysis showed that fungal STSs initiating 1,6 cyclization reaction were apparently grouped into two clades (clade III and clade IV). Apart from metal ion binding motifs, these two clades have no sequence similarity and tend to be conserved in some residues respectively (Figure S6), which may contribute to differences in overall fold of protein structures. It also

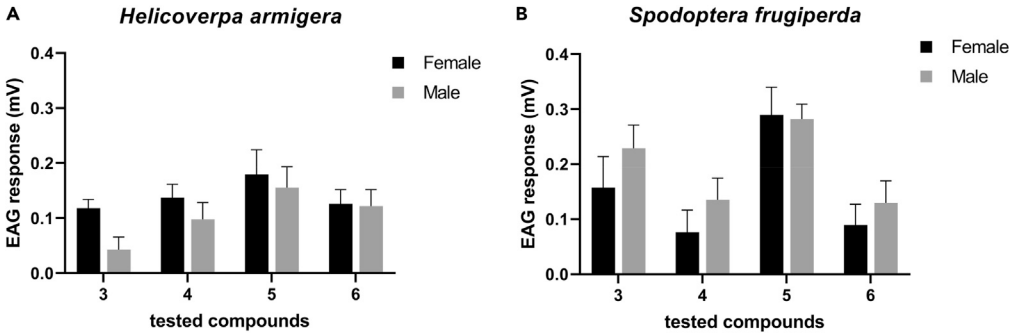

Figure 6. The EAG responses (mV) of *Helicoverpa armigera* and *Spodoptera frugiperda* were elicited by (+)-α-*trans*-bergamotene (3), (−)-trichoacorenol (4), (3*R*,6*E*)-nerolidol (5) and (+)-α-bisabolol (6)

The EAG responses are represented as mean ± SEM.

gives a hint that genes of STSs in clade IV may be involved in horizontal gene transfer from basidiomycetes to ascomycetes. Future studies involving these two clades may provide insight into the mechanism and evolution of fungal 1,6 cyclization STSs.

Based on the general stereochemical model for bicyclic monoterpene, it was inferred that the *endo-anti* cyclization in the left-handed helix of FPP formed the (+)-α-*trans*-bergamotene by (6*R*)-bisabolyl cation, which was further supported by our molecular docking results. The superposition of (±)-limonene synthases and substrate analogues complexes revealed that it is likely that the steric hindrance leads to the different conformations which yield the divergent absolute configurations subsequently (Kumar et al., 2017). As a result, the identification of fungal (−)-α-*trans*-bergamotene synthase will probably facilitate the mechanism with more details.

Known as the constituent of plant essential oil, (−)-α-*trans*-bergamotene was found to play a dual role in flowers and leaves of *Nicotiana attenuata*, solving the dilemma when pollinators are also herbivores (Zhou et al., 2017). The EAG results showed that (+)-α-*trans*-bergamotene (**3**) elicited a significantly higher response of females than males of *H. armigera*, which signified that **3** can potentially attract female moths to oviposit suggesting its potential in biocontrol of *H. armigera*. More behavioral orientation-based assays are underway.

Fungal SRE has been known to be insensitive to the inhibitors (compounds encoded by BGC) and enable the producing organism to survive, illustrating that the SRE in the BGC can serve as a predictive window to the bioactivity of the natural product (Yan et al., 2020). Some representative examples of SREs including the herbicide target AstD (Yan et al., 2018), MetAP-2 of fumagillin cluster (Lin et al., 2013), and HMGR of lovastatin cluster (Kennedy et al., 1999) have been well studied. Our further bioinformatic analysis showed that NecA is the second copy of PIG3 encoded in the genome and has 44% identity with the housekeeping copy PIG3 (scaffold 6) in HLS206, implying that NecA is a variant of housekeeping PIG3. Apart from the *nec* cluster, we observed that the PIG3 variants, NsBERS-like enzymes and cytochrome P450 monooxygenases co-localized in many phytopathogen BGCs (Figure S7), for instance, the *lach* cluster (GenBank: QGMK01000402.1) where LsBERS (TVY81921.1) is located (Figure 2A, Table S5). Based on this, we speculated that the encoded compounds of these BGCs serve as PIG3 inhibitors accelerating infection and plant cell death by regulating the host reactive oxygen species (Peng et al., 2010; Williams et al., 2011). In addition, knocking down PIG3 has been reported to increase the sensitivity of non-small cell lung cancer cells (NSCLC) to docetaxel by dysregulating the dynamics of microtubules (Li et al., 2017), signifying that the putative PIG3 inhibitor compounds **1** and **2** may be potential adjuvants of docetaxel for NSCLC. We will be committed to confirming these potential bioactivities and revealing the underlying mechanisms.

Limitations of the study

In this study, we deciphered the biosynthesis of unusual (2*R*,6*R*)-α-*trans*-bergamotene, and proposed the cyclization mechanism which was supported by molecular docking. However, the docking results did not present the completely symmetrical state because of the differences between plant-derived STSs and fungus-derived STSs in overall fold, especially in active cavity. In addition, in comparison with the protein crystal structure analysis, homology modeling and molecular docking have limitations and are not precise

enough for some details. Therefore, it is hard to predict which residue was the determinant of absolute configuration. Thus, the crystalization and three-dimensional analysis of both two types of enantiomeric synthases and their enzyme-substrate complexes will facilitate the enzymatic mechanism deciphering with more details.

STAR★METHODS

Detailed methods are provided in the online version of this paper and include the following:

- KEY RESOURCES TABLE
- RESOURCE AVAILABILITY
  - Lead contact
  - Materials availability
  - Data and code availability
- EXPERIMENTAL MODEL AND SUBJECT DETAILS
  - Strain and culture conditions
- METHOD DETAILS
  - General experimental procedures
  - Extraction and isolation
  - In silico analysis
  - Heterologous expression in *A. nidulans* A1145 and *S. cerevisiae* BJ5464
  - Plasmid construction of *E. coli* overexpression
  - Protein purification and *in vitro* assays
  - EAG assays
- QUANTIFICATION AND STATISTICAL ANALYSIS

SUPPLEMENTAL INFORMATION

Supplemental information can be found online at https://doi.org/10.1016/j.isci.2022.104030.

ACKNOWLEDGMENTS

We thank Prof. Yi Tang from the University of California, Los Angeles, for providing *Aspergillus nidulans* heterologous expression host and the related plasmids. We acknowledge Prof. Guirong Wang from CAAS for his guidance in the insect pheromone assays. We also thank Prof. Meirong Jia from CAMS & PUMC for critical reading of the manuscript. We are grateful to the Department of Instrumental Analysis of our institute for measurement of the IR, NMR, and MS data. We acknowledge the State Key Laboratory of Natural and Biomimetic Drugs of Peking University School of Pharmaceutical Sciences for measurement of the X-Ray crystallography data. This work is supported by the National Key Research and Development Program of China (grant No. 2018YFA0901900), PUMC Graduate Innovation Fund Project (No. 2019-1007-04, China), PUMC Disciplinary Development of Synthetic Biology (201920100801, China), and CAMS Innovation Fund for Medical Sciences (No. CIFMS2021-I2M-1-029).

AUTHOR CONTRIBUTIONS

Y.H.W. designed and performed the experiments and drafted the manuscript. T.J.C., J.J.C., and F.P. helped for molecular docking. L.Y.J. and Y.P. provided assistance in the experiments. L.L. performed CD measurements. M.G. conducted EAG assays. R.S.W. took part in partial chemical work. J.L.Y. discussed the experimental results, commented on and proofread the manuscript. T.G. designed and performed the chemical work, drafted and revised the manuscript. P.Z. conceived, designed, and supervised the study and revised the manuscript. All authors approved the final manuscript.

DECLARATION OF INTERESTS

The authors declare no competing interests.

Received: August 19, 2021
Revised: January 19, 2022
Accepted: March 2, 2022
Published: April 15, 2022

REFERENCES

Agger, S., Lopez-Gallego, F., and Schmidt-Dannert, C. (2009). Diversity of sesquiterpene synthases in the basidiomycete *Coprinus cinereus*. Mol. Microbiol. *72*, 1181–1195.

Bian, G., Han, Y., Hou, A., Yuan, Y., Liu, X., Deng, Z., and Liu, T. (2017). Releasing the potential power of terpene synthases by a robust precursor supply platform. Metab. Eng. *42*, 1–8.

Bian, G., Hou, A., Yuan, Y., Hu, B., Cheng, S., Ye, Z., Di, Y., Deng, Z., and Liu, T. (2018). Metabolic engineering-based rapid characterization of asesquiterpene cyclase and the skeletons of fusariumdiene and fusagramineol from *Fusarium graminearum*. Org. Lett. *20*, 1626–1629.

Blin, K., Wolf, T., Chevrette, M.G., Lu, X., Schwalen, C.J., Kautsar, S.A., Suarez Duran, H.G., de Los Santos, E.L.C., Kim, H.U., Nave, M., et al. (2017). antiSMASH 4.0-improvements in chemistry prediction and gene cluster boundary identification. Nucleic Acids Res. *45*, W36–W41.

Brill, Z.G., Condakes, M.L., Ting, C.P., and Maimone, T.J. (2017). Navigating the chiral pool in the total synthesis of complex terpene natural products. Chem. Rev. *117*, 11753–11795.

Brock, N.L., and Dickschat, J.S. (2011). Enantioselective synthesis of the unnatural enantiomers of the fungal sesquiterpenoids acorenone and trichoacorenol. Eur. J. Org. Chem. *2011*, 5167–5175.

Brock, N.L., Huss, K., Tudzynski, B., and Dickschat, J.S. (2013). Genetic dissection of sesquiterpene biosynthesis by *Fusarium fujikuroi*. Chembiochem *14*, 311–315.

Cane, D.E., Ha, H.-J., McIlwaine, D.B., and Pascoe, K.O. (1990a). The synthesis of (3*R*)-nerolidol. Tetrahedron Lett. *31*, 7553–7554.

Cane, D.E., McIlwaine, D.B., and Oliver, J.S. (1990b). Absolute configuration of (-)-*β*-*trans*-bergamotene. J. Am. Chem. Soc. *112*, 1285–1286.

Chan, W.K., Tan, L.T., Chan, K.G., Lee, L.H., and Goh, B.H. (2016). Nerolidol: asesquiterpene alcohol with multi-faceted pharmacological and biological activities. Molecules *21*, 259.

Chapuis, C., Barthe, M., Muller, B.L., and Schulte-Elte, K.H. (1998). Preparation and absolute configuration of (-)-(*E*)-*α*-*trans*-Bergamotenone. Helvetica Chim. Acta. *81*, 153–162.

Chen, X.J., Archelas, A., and Furstoss, R. (2002). Microbiological transformations. 27. The first examples for preparative-scale enantioselective or diastereoselective epoxide hydrolyses using microorganisms. An unequivocal access to all four bisabolol stereoisomers. J. Org. Chem. *58*, 5528–5532.

Christianson, D.W. (2008). Unearthing the roots of the terpenome. Curr. Opin. Chem. Biol. *12*, 141–150.

Christianson, D.W. (2017). Structural and chemical Biology of terpenoid cyclases. Chem. Rev. *117*, 11570–11648.

Cistola, D.P., Small, D.M., and Hamilton, J.A. (1982). Ionization behavior of aqueous short-chain carboxylic acids: a carbon-13 NMR study. J. Lipid Res. *23*, 795–799.

Coates, R.M., Denissen, J.F., Juvik, J.A., and Babka, B.A. (1988). Identification of *α*-santalenoic and *endo*-*β*-bergamotenoic acids as moth oviposition stimulants from wild tomato leaves. J. Org. Chem. *53*, 2186–2192.

Croteau, R. (1987). Biosynthesis and catabolism of monoterpenoids. Chem. Rev. *87*, 929–954.

Croteau, R., and Satterwhite, D.M. (1989). Biosynthesis of monoterpenes. J. Biol. Chem. *264*, 15309–15315.

Dixit, M., Weitman, M., Gao, J., and Major, D.T. (2017). Chemical control in the battle against fidelity in promiscuous natural product biosynthesis: the case of trichodiene synthase. ACS Catal. *7*, 812–818.

Gibson, T.W., and Erman, W.F. (1969). Syntheses of the (-)-*α*-and (+)-*β*-*cis*-bergamotenes. J. Am. Chem. Soc. *91*, 4771–4778.

Giroux, E., and Bilodeau, G.J. (2020). Whole genome sequencing resource of the European larch canker pathogen *Lachnellula willkommii* for molecular diagnostic marker development. Phytopathology *110*, 1255–1259.

Gnther, K., Carle, R., Fleischhauer, I., and Merget, S. (1993). Semi-preparative liquid-chromatographic separation of all four stereoisomers of *α*-bisabolol on tribenzoylcellulose. Fresenius J. Anal. Chem. *345*, 787–790.

Guo, M., Du, L., Chen, Q., Feng, Y., Zhang, J., Zhang, X., Tian, K., Cao, S., Huang, T., Jacquin-Joly, E., et al. (2021). Odorant receptors for detecting flowering plant cues are functionally conserved across moths and butterflies. Mol. Biol. Evol. *38*, 1413–1427.

Havlickova, J., Dolejsova, K., Tichy, M., Vrkoslav, V., Kalinova, B., Kyjakova, P., and Hanus, R. (2019). (3*R*,6*E*)-nerolidol, a fertility-related volatile secreted by the queens of higher termites (Termitidae: syntermitinae). Z. Naturforsch. C J. Biosci. *74*, 251–264.

He, H., Bian, G., Herbst-Gervasoni, C.J., Mori, T., Shinsky, S.A., Hou, A., Mu, X., Huang, M., Cheng, S., Deng, Z., et al. (2020). Discovery of the cryptic function of terpene cyclases as aromatic prenyltransferases. Nat. Commun. *11*, 3958.

Jindal, G., and Sunoj, R.B. (2012). Revisiting sesquiterpene biosynthetic pathways leading to santalene and its analogues: a comprehensive mechanistic study. Org. Biomol. Chem. *10*, 7996–8006.

Jones, C.G., Moniodis, J., Zulak, K.G., Scaffidi, A., Plummer, J.A., Ghisalberti, E.L., Barbour, E.L., and Bohlmann, J. (2011). Sandalwood fragrance biosynthesis involves sesquiterpene synthases of both the terpene synthase (TPS)-a and TPS-b subfamilies, including santalene synthases. J. Biol. Chem. *286*, 17445–17454.

Kampranis, S.C., Ioannidis, D., Purvis, A., Mahrez, W., Ninga, E., Katerelos, N.A., Anssour, S., Dunwell, J.M., Degenhardt, J., Makris, A.M., et al. (2007). Rational conversion of substrate and product specificity in a *Salvia* monoterpene synthase: structural insights into the evolution of terpene synthase function. Plant Cell *19*, 1994–2005.

Kanchiswamy, C.N., Malnoy, M., and Maffei, M.E. (2015). Chemical diversity of microbial volatiles and their potential for plant growth and productivity. Front Plant Sci. *6*, 151.

Katoh, K., Misawa, K., Kuma, K., and Miyata, T. (2002). MAFFT: a novel method for rapid multiple sequence alignment based on fast Fourier transform. Nucleic Acids Res. *30*, 3059–3066.

Kennedy, J., Auclair, K., Kendrew, S.G., Park, C., Vederas, J.C., and Hutchinson, C.R. (1999). Modulation of polyketide synthase activity by accessory proteins during lovastatin biosynthesis. Science *284*, 1368–1372.

Kumar, R.P., Morehouse, B.R., Matos, J.O., Malik, K., Lin, H., Krauss, I.J., and Oprian, D.D. (2017). Structural characterization of early michaelis complexes in the reaction catalyzed by (+)-Limonene synthase from *Citrus sinensis*using fluorinated substrate analogues. Biochemistry *56*, 1716–1725.

Kumar, S., Stecher, G., and Tamura, K. (2016). MEGA7: molecular evolutionary genetics analysis version 7.0 for bigger datasets. Mol. Biol. Evol. *33*, 1870–1874.

Landmann, C., Fink, B., Festner, M., Dregus, M., Engel, K.H., and Schwab, W. (2007). Cloning and functional characterization of three terpene synthases from lavender (*Lavandula angustifolia*). Arch. Biochem. Biophys. *465*, 417–429.

Laurini, E., Andreani, S., Muselli, A., Pricl, S., and Tintaru, A. (2020). Direct identification of *α*-bisabolol enantiomers in an essential oilusing a combined ion mobility-mass spectrometry/ quantum chemistry approach. J. Nat. Prod. https://doi.org/10.1021/acs.jnatprod.9b00982.

Li, M., Li, S., Liu, B., Gu, M.M., Zou, S., Xiao, B.B., Yu, L., Ding, W.Q., Zhou, P.K., Zhou, J., et al. (2017). PIG3 promotes NSCLC cell mitotic progression and is associated with poor prognosis of NSCLC patients. J. Exp. Clin. Cancer Res. *36*, 39.

Li, Y., Zhang, F., Banakar, S., and Li, Z. (2019). Bortezomib-induced new bergamotene derivatives xylariterpenoids H–K from sponge-derived fungus *Pestalotiopsis maculans* 16F-12. RSC Adv. *9*, 599–608.

Lin, H.C., Chooi, Y.H., Dhingra, S., Xu, W., Calvo, A.M., and Tang, Y. (2013). The fumagillin biosynthetic gene cluster in *Aspergillus fumigatus* encodes a cryptic terpene cyclase involved in the formation of *β*-*trans*-bergamotene. J. Am. Chem. Soc. *135*, 4616–4619.

Liu, W.C., Li, C.Q., Zhu, P., Yang, J.L., and Cheng, K.D. (2010). Phylogenetic diversity of culturable fungi associated with two marine sponges: *Haliclona simulans* and *Gelliodes carnosa*, collected from the Hainan Island coastal waters of the South China Sea. Fungal Divers. *42*, 1–15.

Lopez-Gallego, F., Agger, S.A., Abate-Pella, D., Distefano, M.D., and Schmidt-Dannert, C. (2010). Sesquiterpene synthases Cop4 and Cop6 from

Coprinus cinereus: catalytic promiscuity and cyclization of farnesyl pyrophosphate geometric isomers. Chembiochem *11*, 1093–1106.

Lu, S., Wang, J., Chitsaz, F., Derbyshire, M.K., Geer, R.C., Gonzales, N.R., Gwadz, M., Hurwitz, D.I., Marchler, G.H., Song, J.S., et al. (2020). CDD/SPARCLE: the conserved domain database in 2020. Nucleic Acids Res. *48*, D265–D268.

Mason, M.G., and Schnepp, O. (1973). Absorption and circular dichroism spectra of ethylenic chromophores-*trans*-cyclooctene, α- and β-pinene. J. Chem. Phys. *59*, 1092–1098.

Max, J.-J., and Chapados, C. (2004). Infrared spectroscopy of aqueous carboxylic acids: comparison between different acids and their salts. J. Phys. Chem. A *108*, 3324–3337.

Miller, D.J., and Allemann, R.K. (2012). Sesquiterpene synthases: passive catalysts or active players? Nat. Prod. Rep. *29*, 60–71.

Muangphrom, P., Misaki, M., Suzuki, M., Shimomura, M., Suzuki, H., Seki, H., and Muranaka, T. (2019). Identification and characterization of (+)-alpha-bisabolol and 7-*epi*-silphiperfol-5-ene synthases from *Artemisia abrotanum*. Phytochemistry *164*, 144–153.

Muangphrom, P., Seki, H., Suzuki, M., Komori, A., Nishiwaki, M., Mikawa, R., Fukushima, E.O., and Muranaka, T. (2016). Functional analysis of amorpha-4,11-diene synthase (ADS) homologs from non-artemisinin-producing Artemisia species: the discovery of novel koidzumiol and (+)-alpha-Bisabolol synthases. Plant Cell Physiol. *57*, 1678–1688.

Oh, H., Gloer, J.B., and Shearer, C.A. (1999). Massarinolins A-C: new bioactive sesquiterpenoids from the aquatic fungus *massarina tunicata*. J. Nat. Prod. *62*, 497–501.

Ohashi, M., Liu, F., Hai, Y., Chen, M., Tang, M.C., Yang, Z., Sato, M., Watanabe, K., Houk, K.N., and Tang, Y. (2017). SAM-dependent enzyme-catalysed pericyclic reactions in natural product biosynthesis. Nature *549*, 502–506.

Peng, X.L., Xu, W.T., Wang, Y., Huang, K.L., Liang, Z.H., Zhao, W.W., and Luo, Y.B. (2010). Mycotoxin Ochratoxin A-induced cell death and changes in oxidative metabolism of *Arabidopsis thaliana*. Plant Cell Rep. *29*, 153–161.

Peralta-Yahya, P.P., Ouellet, M., Chan, R., Mukhopadhyay, A., Keasling, J.D., and Lee, T.S. (2011). Identification and microbial production of a terpene-based advanced biofuel. Nat. Commun. *2*, 483.

Porte, S., Valencia, E., Yakovtseva, E.A., Borras, E., Shafqat, N., Debreczeny, J.E., Pike, A.C.W., Oppermann, U., Farres, J., Fita, I., et al. (2009). Three-dimensional structure and enzymatic function of proapoptotic human p53-inducible quinone oxidoreductase PIG3. J. Biol. Chem. *284*, 17194–17205.

Quin, M.B., Flynn, C.M., and Schmidt-Dannert, C. (2014). Traversing the fungal terpenome. Nat. Prod. Rep. *31*, 1449–1473.

Rinkel, J., and Dickschat, J.S. (2020). Mechanistic studies on trichoacorenol synthase from *Amycolatopsis benzoatilytica*. Chembiochem *21*, 807–810.

Sallaud, C., Rontein, D., Onillon, S., Jabes, F., Duffe, P., Giacalone, C., Thoraval, S., Escoffier, C., Herbette, G., Leonhardt, N., et al. (2009). A novel pathway for sesquiterpene biosynthesis from *Z,Z*-farnesyl pyrophosphate in the wild tomato *Solanum habrochaites*. Plant Cell *21*, 301–317.

Schnee, C., Kollner, T.G., Gershenzon, J., and Degenhardt, J. (2002). The maize gene terpene synthase 1 encodes a sesquiterpene synthase catalyzing the formation of (*E*)-beta-farnesene, (*E*)-nerolidol, and (*E,E*)-farnesol after herbivore damage. Plant Physiol. *130*, 2049–2060.

Shaw, J.J., Berbasova, T., Sasaki, T., Jefferson-George, K., Spakowicz, D.J., Dunican, B.F., Portero, C.E., Narvaez-Trujillo, A., and Strobel, S.A. (2015). Identification of a fungal 1,8-cineole synthase from *Hypoxylon* sp. with specificity determinants in common with the plant synthases. J. Biol. Chem. *290*, 8511–8526.

Sy, L.-K., and Brown, G.D. (1997). Total assignment of the ^{1}H and ^{13}C NMR chemical shifts of three bisabolane hydrocarbons by 2D-NMR spectroscopy. Magn. Reson. Chem. *35*, 424–425.

Tantillo, D.J. (2011). Biosynthesis via carbocations: theoretical studies on terpene formation. Nat. Prod. Rep. *28*, 1035–1053.

Trott, O., and Olson, A.J. (2010). AutoDock Vina: improving the speed and accuracy of docking with a new scoring function, efficient optimization, and multithreading. J. Comput. Chem. *31*, 455–461.

Van Kan, J.A., Stassen, J.H., Mosbach, A., Van Der Lee, T.A., Faino, L., Farmer, A.D., Papasotiriou, D.G., Zhou, S., Seidl, M.F., Cottam, E., et al. (2017). A gapless genome sequence of the fungus *Botrytis cinerea*. Mol. Plant Pathol. *18*, 75–89.

Wang, Y.N., Xia, G.Y., Wang, L.Y., Ge, G.B., Zhang, H.W., Zhang, J.F., Wu, Y.Z., and Lin, S. (2018). Purpurolide A, 5/5/5 spirocyclic sesquiterpene lactone in nature from the endophytic fungus *Penicillium purpurogenum*. Org. Lett. *20*, 7341–7344.

Waterhouse, A., Bertoni, M., Bienert, S., Studer, G., Tauriello, G., Gumienny, R., Heer, F.T., de Beer, T.A.P., Rempfer, C., Bordoli, L., et al. (2018). SWISS-MODEL: homology modelling of protein structures and complexes. Nucleic Acids Res. *46*, W296–W303.

Wawrzyn, G.T., Quin, M.B., Choudhary, S., Lopez-Gallego, F., and Schmidt-Dannert, C. (2012). Draft genome of *Omphalotus olearius* provides a predictive framework for sesquiterpenoid natural product biosynthesis in Basidiomycota. Chem. Biol. *19*, 772–783.

Whittington, D.A., Wise, M.L., Urbansky, M., Coates, R.M., Croteau, R.B., and Christianson, D.W. (2002). Bornyl diphosphate synthase: structure and strategy for carbocation manipulation by a terpenoid cyclase. Proc. Natl. Acad. Sci. U S A. *99*, 15375–15380.

Williams, B., Kabbage, M., Kim, H.J., Britt, R., and Dickman, M.B. (2011). Tipping the balance: *Sclerotinia sclerotiorum* secreted oxalic acid suppresses host defenses by manipulating the host redox environment. PLoS Pathog. *7*, e1002107.

Yan, D., Chen, Q., Gao, J., Bai, J., Liu, B., Zhang, Y., Zhang, L., Zhang, C., Zou, Y., and Hu, Y. (2019). Complexity and diversity generation in the biosynthesis of fumiquinazoline-related peptidyl alkaloids. Org. Lett. *21*, 1475–1479.

Yan, Y., Liu, N., and Tang, Y. (2020). Recent developments in self-resistance gene directed natural product discovery. Nat. Prod. Rep. *37*, 879–892.

Yan, Y., Liu, Q., Zang, X., Yuan, S., Bat-Erdene, U., Nguyen, C., Gan, J., Zhou, J., Jacobsen, S.E., and Tang, Y. (2018). Resistance-gene-directed discovery of a natural-product herbicide with a new mode of action. Nature *559*, 415–418.

Ying, Y.M., Fang, C.A., Yao, F.Q., Yu, Y., Shen, Y., Hou, Z.N., Wang, Z., Zhang, W., Shan, W.G., and Zhan, Z.J. (2017). Bergamotane sesquiterpenes with alpha-glucosidase inhibitory activity from the plant pathogenic fungus *Penicillium expansum*. Chem. Biodivers *14*, e1600184.

Zhang, C., Chen, X., Orban, A., Shukal, S., Birk, F., Too, H.P., and Ruhl, M. (2020). *Agrocybe aegerita*serves as a gateway for identifying sesquiterpene biosynthetic enzymes in higher fungi. ACS Chem. Biol. *15*, 1268–1277.

Zhou, W., Kugler, A., McGale, E., Haverkamp, A., Knaden, M., Guo, H., Beran, F., Yon, F., Li, R., Lackus, N., et al. (2017). Tissue-specific emission of (*E*)-alpha-Bergamotene helps resolve the dilemma when pollinators are also herbivores. Curr. Biol. *27*, 1336–1341.

STAR★METHODS

KEY RESOURCES TABLE

REAGENT or RESOURCE	SOURCE	IDENTIFIER
Strains		
Nectria sp. HLS206	Lab stock	N/A
Aspergillus nidulans	(Ohashi et al., 2017)	A1145
Saccharomyces cerevisiae	(Ohashi et al., 2017)	BJ5464
E. coli T1	Transgen biotech	Cat# CD501-03
E. coli BL21(DE3)	Transgen biotech	Cat# CD601-03
Chemicals, peptides, and recombinant proteins		
GPP	Sigma-Aldrich	Cat# G6772
FPP	Sigma-Aldrich	Cat# F6892
GGPP	Sigma-Aldrich	Cat# G6025
Critical commercial assays		
Fungal RNA Kit	Omega Bio-tek	Cat# R6840-01
cDNA Synthesis Kit	Transgen biotech	Cat# AE311-02
Q5 high fidelity DNA polymerase	NEB	Cat# M0491L
Zymoprep Yeast Miniprep Kit	Zymo Research	Cat# D2001
recombinase Exnase II	Vazyme Biotech	Cat# C112
Deposited data		
CIF of compound 1	this paper	CCDC: 2098349
nec cluster *necA*	this paper	GenBank: MZ672110
nec cluster *necB*	this paper	GenBank: MZ672111
nec cluster *necC*	this paper	GenBank: MZ672112
nec cluster necD	this paper	GenBank: MZ672113
nec cluster necE	this paper	GenBank: MZ672114
nec26	this paper	GenBank: MZ672115
Oligonucleotides		
For details of oligonucleotides generated and used, see Table S7	this work	N/A
Recombinant DNA		
For details of plasmids generated and used, see Table S8	this work	N/A
Software and algorithms		
MAFFT	(Katoh et al., 2002)	https://mafft.cbrc.jp/alignment/software/
MEGA7	(Kumar et al., 2016)	https://www.megasoftware.net/
2ndFind	N/A	https://biosyn.nih.go.jp/2ndfind/
NCBI conserved domain database	(Lu et al., 2020)	https://www.ncbi.nlm.nih.gov/cdd
SWISS-MODEL	(Waterhouse et al., 2018)	https://swissmodel.expasy.org/
AutoDock Vina	(Trott and Olson, 2010)	http://vina.scripps.edu/

RESOURCE AVAILABILITY

Lead contact

Further requests for information should be addressed to Ping Zhu at zhuping@imm.ac.cn.

Materials availability

Requests for materials should be made via the lead contact.

Data and code availability

The crystallographic information file (CIF) of compound **1** was deposited into Cambridge Crystallographic Data Center with the deposition number 2098349. The *nec* cluster (*necA-necE*) were deposited into the GenBank with the accession number MZ672110~MZ672114. The *nec*26 was deposited into the GenBank under the accession number MZ672115.

A summary of analysis software and tools were provided in key resources table. This paper does not report original code.

Any additional information required to reanalyze the data reported in this paper is available from the lead contact upon request.

EXPERIMENTAL MODEL AND SUBJECT DETAILS

Strain and culture conditions

Nectria sp. HLS206 isolated from the marine sponge *Gelliodas carnosa* (Liu et al., 2010) and deposited at our laboratory was cultured in rice medium for isolation compounds **1** and **2**. After 3 days of culturing in YPD medium, the gDNA of *Nectria* sp. HLS206 was isolated by CTAB for next generation sequencing. *E. coli* T1 was used for plasmid construction and *E. coli* BL21(DE3) was used for protein expression. *A. nidulans* A1145 and *S. cerevisiae* BJ5464 were used for heterologous expression.

METHOD DETAILS

General experimental procedures

Optical rotations were recorded using a Rudolph Research Analytical automatic polarimeter (Rudolph Research Analytical, Hackettstown, NJ, USA). Circular dichroism (CD) was measured on a JASCO J-815 CD spectro polarimeters (JASCO Corporation, Tokyo, Japan). IR spectra were acquired by KBr disk method on a Shimadzu FTIR-8400S spectrometer (Shimadzu Co. Ltd., Tokyo, Japan). 1D and 2D nuclear magnetic resonance (NMR) spectra were recorded on a Bruker AV-500 spectrometer (Bruker Biospin Group, Karlsruhe, Germany) with TMS as an internal standard. Mass spectra were measured on Thermo Scientific Q Exactive Focus Orbitrap mass spectrometer (Waltham, MA, USA) for HRESIMS. GC-MS analysis was conducted by GCMS-TQ8050 (Shimadzu Co. Ltd., Tokyo, Japan) using the Rtx-5MS column (30 m × 0.25 mm × 0.25 μm).

Semi-preparative HPLC was conducted on an Agilent C18 column (250 × 10 mm I.D., 5 μm) equipped with a LC-6AD pump and a Shimadzu SPD-20A UV-Vis detector (Shimadzu Co. Ltd., Japan). Column chromatography (CC) was performed with silica gel (100–200 and 200–300 mesh, Qingdao Marine Chemical plant, Qing dao, China), ODS-C18 (50 μm, YMC Co. Ltd., Kyoto, Japan), and Sephadex LH-20 (18–110 μm, GE healthcare, Fairfield, CT, USA). Chromatographic or analytical grade solvents were used for isolation and separation procedures.

Extraction and isolation

The EtOAc extract (28.2 g) of the rice solid cultures of fungus HLS206 (5 kg) was first separated using ODS column, and eluted successively with 20%, 30%, 40%, 50%, 60%, 80% and 100% CH_3OH in H_2O to produce eight fractions (Fr. 1–8). Fr.4 was subjected to Sephadex LH-20 column eluted by CH_3OH to give 16 subfractions (Fr. 4.1–4.16). Compounds **2′** (7.1 mg, Rt 24 min) and **2** (40.8 mg, Rt 36 min) were obtained from Fr. 4.9 through semi-preparative HPLC eluted by 30% CH_3CN-H_2O. From Fr. 4.12, we obtained compound **1** (23.6 mg, Rt 21 min) by semi-preparative HPLC, eluted by gradient CH_3CN-H_2O (0 min, 20%-10 min, 40%-30 min, 80%).

For purification of compounds **3**–**6**, the *n*-octane layers were concentrated using a rotary evaporator, and terpenoids were purified using semi-preparative HPLC with acetonitrile and water as the mobile phase (Bian et al., 2018). The GC-MS procedure was described as previous research (Bian et al., 2017).

Necbergamotenoic acid A (**1**): colorless crystals; $[\alpha]^{20}{}_{D}$ +51.5 (*c* 0.2, CH_3OH); CD (*c* 0.1(w/v)%, CH_3OH) 218.5 (2.44) nm, Figure S16; IR (KBr) ν_{max} 3039, 2985, 2963, 2933, 2660, 1697, 1674, 1640, 1427, 1289, 1255, 926, 802, 739, 708, 573 cm^{-1}, Figure S9; ^1H NMR ($CDCl_3$, 500 MHz) and ^{13}C NMR ($CDCl_3$, 125 MHz) data, Table 1; (+)-HR-ESI-MS *m/z* 287.1246 $[M + Na]^+$ (calcd for $C_{15}H_{20}O_4Na$ 287.1254).

Necbergamotenoic acid B (**2**): yellowish gum; $[\alpha]^{20}{}_{D}$ +100.9 (*c* 0.2, CH_3OH); CD (*c* 0.4(w/v)%, CH_3OH) 215.5 (5.46) nm, Figure S25; IR (KBr) ν_{max} 3271, 2931, 2840, 2688, 1692, 1650, 1438, 1249, 1026, 791, 754, 662 cm^{-1}, Figure S18; ^1H NMR (CD_3OD, 500 MHz) and ^{13}C NMR (CD_3OD, 125 MHz) data, Table 1; (+)-HR-ESI-MS *m/z* 289.1405 $[M + Na]^+$ (calcd for $C_{15}H_{22}O_4Na$ 289.1410).

Ionized form of Necbergamotenoic acid B (**2'**): yellowish gum; IR (KBr) ν_{max} 3271(w), 2971(w), 2924(w), 1573(s), 1426(s), 1042, 1014, 924,781, 649, 620 cm^{-1}, Figure S27; ^1H NMR (CD_3OD, 500 MHz) and ^{13}C NMR (CD_3OD, 125 MHz) data, Table 1; (+)-HR-ESI-MS *m/z* 289.1403 $[M]^+$ (calcd for $C_{15}H_{22}O_4Na$ 289.1410).

(+)-α-trans-bergamotene (**3**): colorless oil; $[\alpha]^{20}{}_{D}$ +22.5 (*c* 0.2, $CHCl_3$); CD (*c* 0.1(w/v)%, *n*-hexane) 209 (0.70) nm, Figure S37; IR (KBr) ν_{max} 3380, 2954, 2924, 2955, 1725, 1461, 1377, 1263, 1223, 1077, 1026, 973, 799, 740 cm^{-1}, Figure S34; ^1H NMR ($CDCl_3$, 500 MHz) and ^{13}C NMR ($CDCl_3$, 125 MHz) data, Table S2; GC-MS, Figure 2B.

(−)-trichoacorenol (**4**): colorless oil; $[\alpha]^{20}{}_{D}$ −6 (*c* 0.1, $CHCl_3$); ^1H NMR ($CDCl_3$, 500 MHz): 5.46 (m, H-2), 4.27 (m, H-4), 0.83 (d, *J* = 6.5 Hz, CH_3-12), 0.93 (d, *J* = 6.5 Hz, CH_3-13), 0.82 (d, *J* = 6.5 Hz, CH_3-14), 1.77 (brs, CH_3-15); ^{13}C NMR ($CDCl_3$, 125 MHz) data, Table S3; GC-MS, Figure 2B.

(3R)-nerolidol (**5**): colorless oil; $[\alpha]^{20}{}_{D}$ −16 (*c* 0.1, $CHCl_3$); ^1H NMR ($CDCl_3$, 500 MHz): 5.92 (dd, *J* = 18.0, 11.0 Hz, H-2), 5.22 (dd, *J* = 18.0 Hz, H-1a), 5.07 (dd, *J* = 11.0 Hz, H-1b), 5.15 (t, *J* = 6.5 Hz, H-6), 5.09 (t, *J* = 6.5 Hz, H-10), 1.27 (d, CH_3-12), 1.59 (s, CH_3-13, CH_3-15), 1.59 (d, CH_3-14), 1.67 (brs, CH_3-15); ^{13}C NMR ($CDCl_3$, 125 MHz) data, Table S3; GC-MS, Figure 4B.

(+)-α-bisabolol (**6**): colorless oil; $[\alpha]^{20}{}_{D}$ +51.7 (*c* 0.06, $CHCl_3$); ^1H NMR ($CDCl_3$, 500 MHz) 5.37 (m, H-2), 5.12 (t, *J* = 6.8 Hz, H-10), 1.62 (s, CH_3-12), 1.68 (s, CH_3-13), 1.10 (s, CH_3-14), 1.64 (s, CH_3-15); ^{13}C NMR ($CDCl_3$, 125 MHz) data, Table S3; GC-MS, Figure 4B.

In silico analysis

For phylogenetic analysis, the multiple sequence alignment was generated using MAFFT and phylogenetic tree was generated in MEGA7 using Neighbor-Joining method based on the poisson model. The parameter of *Gamma* Distributed was set as 3 and pairwise deletion was adopted in missing data treatment. The gene annotation results were generated by 2ndFind and NCBI conserved domain database. Homology modelling was conducted by SWISS-MODEL. The molecular docking was generated by AutoDock Vina and visualized using PyMOL.

Heterologous expression in *A. nidulans* A1145 and *S. cerevisiae* BJ5464

The plasmids pYTU-Nec04, pYTU-NecD and pYTU-Nec26 for *A. nidulans* expression were assembled by yeast homologous recombination (Ohashi et al., 2017). The genes *nec04*, *necD* and *nec26* carrying ~200 bp terminators were amplified from the gDNA of HLS206 using primers pYTU-Nec04-F/R, pYTU-NecD-F/R and pYTU-Nec26-F/R with flanking regions of pYTU (Table S7). The PCR products and Pac I digested pYTU were co-transformed into *S. cerevisiae* BJ5464. The plasmid was extracted from yeast using Zymoprep Yeast Miniprep Kit and transformed to *E. coli* T1 for sequencing. Preparation of the protoplast and transformation of *A. nidulans* A1145 were performed as previously described (Yan et al., 2019). The transformation mixture was spread on the selected GMM agar medium (10 g/L glucose, 6 g/L $NaNO_3$, 0.52 g/L KCl, 0.52 g/L $MgSO_4{\cdot}7H_2O$, 1.52 g/L KH_2PO_4, 1 mL/L trace elements solution, 20 g/L agar) with 1.2 M sorbitol and supplementation of pyridoxine HCl (0.5 μg/mL) and riboflavin (2.5 μg/mL) (uracil and uridine dropout). After culturing at 37°C for 3 days, the transformants were transferred to fresh GMM plates and cultured for another 3 days. Then the transformants screening was conducted by PCR using primers U-F/R to confirm for the presence of corresponding plasmids. The correct transformants were incubated in 20 mL liquid CD-ST medium (20 g/L starch, 20 g/L tryptone, 6 g/L $NaNO_3$, 0.52 g/L KCl, 0.52 g/L $MgSO_4{\cdot}7H_2O$, 1.52 g/L KH_2PO_4, 1 mL/L trace elements solution) with supplementation of pyridoxine

HCl and riboflavin overlaid with 2 mL *n*-dodacane at 25°C, 180 rpm and the organic layers were detected by GC-MS after 6 days.

The RNA of *A. nidulans* recombinant *AN-necD* was obtained by using Fungal RNA Kit. The One-Step gDNA Removal and cDNA Synthesis Kit was used to synthesize the cDNA. For construction of plasmid pESC-URA-NsBERS, the intron-free *necD* was amplified with overhang primers pESC-URA-NsBERS-F/R from cDNA of *AN-necD* and cloned into pESC-URA (BamH I / Sal I). The genes of LsBERS and BcBOS were chemically synthesized by GeneScript (GenScript USA Inc., Piscataway, NJ, USA) and directly cloned into pESC-URA (BamH I / Sal I) yielding pESC-URA-LsBERS and pESC-URA-BcBOS. The pESC-LEU-*t*HMGR-ERG20 was co-transformed into *S. cerevisiae* BJ5464 with pESC-URA-NsBERS/LsBERS/BcBOS, respectively. The *S. cerevisiae* transformants were incubated in uracil-dropout medium and induced by galactose at 30°C, 220 rpm for 3 days. The *n*-octane organic layers overlaid the medium were detected by GC-MS.

Plasmid construction of *E. coli* overexpression

For construction of pET28a-MBP-NsBERS, the intron-free *necD* was amplified with overhang primers from cDNA using Q5 high fidelity DNA polymerase and cloned into modified pET28a (MBP His6 tagged) using recombinase Exnase II. For construction of pET28a-MBP-LsBERS, the DNA fragment *lachB* was amplified from pESC-URA-LsBERS and cloned into modified pET28a (MBP His6 tagged). For the construction of pET28a-BcBOS, the DNA fragment *bcbos* were ligated into BamH I / Not I digested pET28a.

Protein purification and *in vitro* assays

For protein purification, *E. coli* BL21 (DE3) harboring the expression plasmids were cultivated in 2 L LB medium supplemented with 50 mg/L kanamycin (KAN) at 37°C, 220 rpm until OD_{600} reached 0.4–0.6. After cooling to 16°C, 0.1 mM IPTG was added and the cultures were induced at 16°C, 150 rpm for 16 h. The cells were collected by centrifugation and resuspended in buffer A (50 mM Tris-HCl, 500 mM NaCl, 10% glycerol, pH 7.6) and lysed by sonication on ice. The cellular debris were removed through centrifugation at 12,000 rpm, 4°C for 40 min. The protein was purified by AKTA system using Ni-NTA column (GE Healthcare). The purified protein was then concentrated and preserved in buffer C (50 mM Tris-HCl, 50 mM NaCl, 5% glycerol, pH 7.6) by desalting column (GE Healthcare) for *in vitro* assays.

Unless otherwise stated, the reactions were conducted using 5 μM purified proteins, 100 μM substrates (GPP, FPP or GGPP), and 10 mM Mg^{2+} in 50 μL of reaction buffer (50 mM Tris-HCl buffer, 10% glycerol, pH 7.6) covered 60 μL *n*-dodacane. The reaction mixtures were incubated at 30°C overnight. After centrifugation and dried with anhydrous sodium sulfate, the organic phase was analyzed by GC-MS.

EAG assays

The EAG assays were performed on both sexes of *Helicoverpa armigera* and *Spodoptera frugiperda* respectively according to previous reports (Guo et al., 2021). The antennae of 3-day-old virgin male and female moths were cut at the base of the flagellum. About 1 μg/μL stock solutions of individual compound was prepared with *n*-hexane. In each test, 10 μg of each compound was used for stimulation. Odor stimulation was controlled by a puff of purified air (0.2 s at 10 mL/s airflow) from a stimulus controller (CS-55, Syntech, Kirchzarten, Germany). EAG signals were recorded and monitored with an Intelligent Data Acquisition Controller (IDAC-4-USB, Syntech), then analyzed using Syntech EAG-software. For each compound, 4 or 5 antennae from different individual moths were tested. The EAG response values of each compound were calculated by subtracting that of the same antennae corresponding to a solvent blank of *n*-hexane.

QUANTIFICATION AND STATISTICAL ANALYSIS

In general, data were analyzed in Excel and figures are plotted in GraphPad Prism. Details of replicates and data analysis for each experiment can be found in the figure legends.